AIAA SciTech Forum
23-27 January 2023, National Harbor, MD & Online
AIAA SCITECH 2023 Forum
10.2514/6.2023-2068

A Time-Varying Subspace Method for Shape Estimation of a Flexible Spacecraft Membrane

Matthew Brownell *[1], Andrew Sinclair †[2], and Puneet Singla ‡[1]
[1]*The Pennsylvania State University, University Park, PA, 16802*
[2]*Air Force Research Laboratory, Kirtland AFB, NM, 87117*

The focus of this work is to develop a reduced-order model to capture the motion of a large, flexible spacecraft from distributed sensor measurements. The spacecraft structure is motivated by a concept for capturing solar energy and accurately directing it to desired locations on the Earth's surface. A previously developed analytical model is utilized to simulate data of the fully-coupled attitude-orbital-flexible dynamics of a large spacecraft in orbit. Utilizing this simulation in place of an experimental test-bed, local acceleration sensor measurements, distributed across the surface of the spacecraft, are obtained. This data is then used to find a reduced-order model to estimate the shape of the spacecraft in real-time with lower computational complexity.

Rather than finding a global model between input and output space, system theory concepts are utilized to find a subspace over which the unknown dynamics evolve. This paper utilizes the Eigensystem Realization Algorithm (ERA) to obtain said reduced-order model. The derived reduced-order model is guaranteed to capture controllable and observable modes of the spacecraft motion. The reduced-order model's validity is tested by attempting to replicate the analytical model's output data and dynamic characteristics such as modal frequency and damping. The resultant reduced-order model accurately reproduced the output data and dynamic characteristics of the analytical model. This provides a basis for optimism in identifying flexible-body dynamics from input-output data while in an orbit.

I. Introduction

The accurate and timely supply of energy for the Department of Defense is paramount to mission success. Space-solar power is one concept to address this need via capturing solar energy in space and accurately directing it to required locations on the Earth's surface. The Space Solar Power Incremental Demonstrations and Research Project (SSPIDR) considers deploying large solar arrays as a solution; however, to accurately transmit power, precise knowledge of the dynamic shape of the flexible structure is required [1]. A conceptual design of a SSPIDR spacecraft is shown in Figure 1.

Using a novel "sandwich tile", solar energy is collected via photovoltaic cells, converted to Radio Frequency (RF), and then beamed to a receiving antenna on the ground. The ground station then rectifies the RF beam into usable power. The shape of the spacecraft helps to aim the RF beam onto the receiving antenna. If the RF beam is required to be within centimeters of the ground station, an angle tolerance on the order of micro-degrees is required for the spacecraft's beaming (assuming a Low Earth Orbit). Additionally, vibrations of the structure are of interest and must be minimized in order to maintain pointing accuracy. One concept to measure the structural shape is to utilize sensors over the surface that provide local displacement or slope information. This local data can be utilized to estimate the shape of the spacecraft and therefore apply corrections to the radio-frequency beam formation. This requires the study of flexible-body dynamics coupled with rigid-body dynamics.

Large, flexible structures in space is not a new concept. In 2021, the Air Force Research Laboratory's Demonstration and Science Experiments (DSX) spacecraft served a 23-month mission in which the complex relationship between low-frequency radio waves and the Earth's radiation belts in medium Earth orbit (MEO) was explored [2]. A precision 25 meter boom and 25 meter truss were tested. The long antenna of this spacecraft would vibrate while in orbit and was damped to ensure proper experimentation. Additionally, there is the concept of solar sail in which a large, flexible "sail" utilizes momentum from photons to translate [3]. In 2019, the LightSail 2 spacecraft was launched into orbit and utilizes a 32 m^2 solar sail to resist atmospheric friction in order to stay in orbit [4]. Much like the concept design for SSPIDR, the sail is a large, two-dimensional structure. Although solar sails are typically smaller than what is planned

*Graduate Student, Department of Aerospace Engineering, AIAA Student Member, AAS Student Member, mtb5476@psu.edu
†Senior Aerospace Engineer, AIAA Associate Fellow, AAS Fellow, Space Vehicles Directorate, andrew.sinclair.2@spaceforce.mil
‡Professor, Department of Aerospace Engineering, AIAA Associate Fellow, AAS Fellow, psingla@psu.edu.

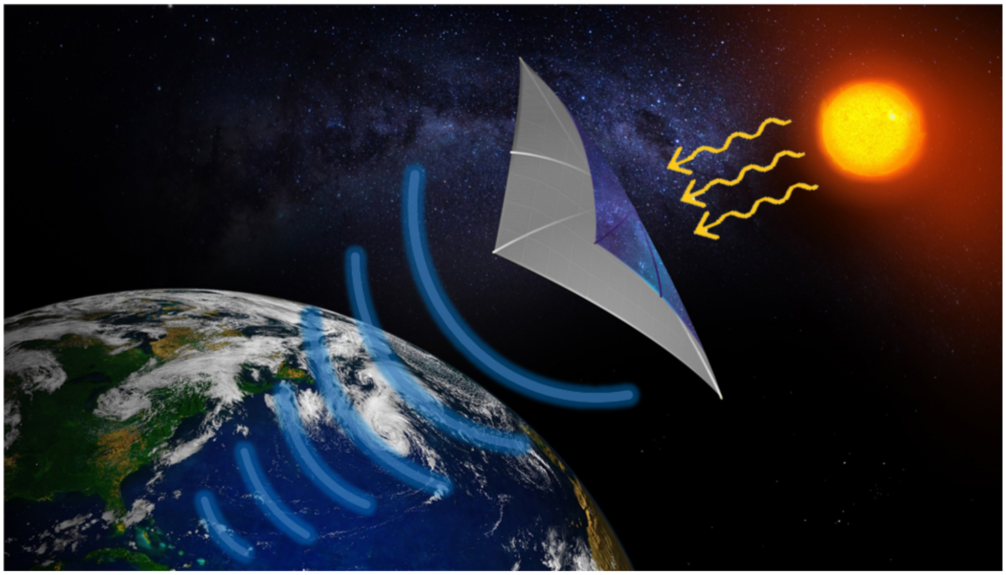

Figure 1 Spacecraft Concept [1]

for SSPIDR (solar sails typically have a surface area $O(10)m^2$ while SSPIDR is expected to be at least $O(100)m^2$), they experience similar challenges with induced vibrations due to translation, rotation, and gravitational effects.

Flexible multi-body systems have been a significant research topic for decades. The work of Meirovich and Stemple [10] from the mid 90s diverges away from classical approximations such as the Rayleigh-Ritz Method and finite-element methods. Instead, a mathematical formulation for distributed-parameter multi-body systems that consists of ordinary and partial differential equations of motion in terms of quasi-coordinates is presented. Similarly, the work of Junkins and Kim [8] provides a Lagrangian framework to derive equations of motion of distributed-parameter multi-body systems. This methodology was utilized previously to produce an analytical model that fully encapsulates the coupled rigid-body, flexible-body, in-orbit dynamics of a large, flexible spacecraft [6].

Although the analytical modeling results are useful for analysis, the simulations' long run-times hinder the practicality of their use in real-time control and decision making. Furthermore, external effects due to change in environment conditions (such as temperature gradients) affect the accuracy of analytical models as they are difficult to model. Hence, there is a need to develop methods which can capture essential dynamics and/or corrections to analytical models from sensor observations. It is desired that such approaches can trade off between accuracy and computation time.

Reduced-order modeling comes from a broader topic referred to as *system identification*, which finds a dynamical model solution for the input-output data collected over time. The output at any given time is considered a function of the input signal, which is also a function of time. Implicitly, one expects the input-output data to be sufficiently rich such that the reduced-order model is accurate over a wide class of inputs and is useful for other purposes such as controlling the system.

Recent advances in machine learning, such as artificial neural networks (ANN), can be used to find a global continuous map from system input space to system output space; however, the performance of these algorithms decreases drastically as the dimension of the system output vector increases. To make this point more clear, consider the problem of active control of a flexible space structure. Generally, the system output vector consists of surface distortion measurements at various spatial points, $O(10^3)$, which are measured by sensors such as strain gauges, slope sensors, stereo vision systems, LIDAR, etc. If one seeks a dynamic continuous map between the system output and input, then the dimension can be as large as the number of measurements, i.e. $O(10^3)$. Conversely, the dimension of the hidden states corresponds to the number of dynamic structural modes of interest, which are typically fewer than 10. Therefore, a system identification algorithm is desired that can approximate the system output accurately while keeping the dimension of the dynamic map as low as possible.

The specific problem of flexible structure control blends concepts from engineering mechanics, control theory, and computational science in order to damp the vibrations detected by sensors on the spacecraft. Working at the confluence of these different disciplines, the engineers of the 90s contributed to many advancements in linear system theory [8]. As a result, the preceding decades led to many works in the time-domain identification of linear systems [9, 11–14].

Ho and Kalman [9] paved the way for minimum realization theory by showing that a minimum dimension state-space model can be achieved by analyzing a sequence of pulse response functions known as Markov parameters. Since then, an extension of the Ho-Kalman algorithm, known as the Eigensystem Realization Algorithm (ERA) [15, 16], has been at the forefront of system identification due to its efficiency and ease of use. ERA provides a minimal-realization of the system based solely on input-output data and allows for further system analysis and control.

In the context of a large, flexible spacecraft, ERA identifies the main vibrational modes excited during a spacecraft's mission and is used for the reduced-order modeling in this paper. In general, there are nonlinear system identification techniques available that represent state-perturbation dynamics for large classes of systems where a linear approximation is not adequate [5, 7]. This is especially true for systems of high state dimension (i.e. large, flexible spacecraft). The work of Junkins and Singla [5] found that linear system identification (via ERA) can perform well in identifying perturbation dynamics. Additionally, the linear model can be combined with nonlinear correction terms to improve fidelity. In this paper, simplifying assumptions are made for the spacecraft model that result in linear equations of motion for the elastic domain. Although this results in a lack of fidelity, the aim is a proof of concept of system identification methods for spacecraft inspired by SSPIDR.

To this effect, the ultimate goal of this paper is to provide evidence for the practicality of system identification methods in the context of large, flexible space structures. As a result, the objective is to use ERA to identify a minimal-realization of the flexible space-based structure from input-output data that allows for further system analysis and control.

In this paper, the previously mentioned high-fidelity coupled rigid-flexible dynamic model is used to simulate the output of acceleration sensors distributed over the surface of the elastic domain of the spacecraft. ERA is then used to find a reduced-order dynamic model from these sensor measurements. Lastly, the reduced-order model is tested for validity by comparing its output and eigenvalues to that of the analytical model.

II. Problem Statement

Consider the coupled rigid-flexible structure in the linear state-space form

$$\dot{\mathbf{z}} = A_c(t)\mathbf{z} + B_c(t)\mathbf{u}, \quad \mathbf{z} \in \mathbb{R}^{n\times 1},\ \mathbf{u} \in \mathbb{R}^{g\times 1} \tag{1}$$

$$\mathbf{y} = C(t)\mathbf{z} + D(t)\mathbf{u}, \quad \mathbf{y} \in \mathbb{R}^{m\times 1}, \tag{2}$$

where $\mathbf{z}$ is the hidden state vector, $\mathbf{y}$ is the output, and $\mathbf{u}$ is the input. A discrete time model corresponding to the solution of (1) can be written as

$$\dot{\mathbf{z}}_{k+1} = A_k\mathbf{z}_k + B_k\mathbf{u}_k, \quad A_k = \Phi(k+1, k) \tag{3}$$

$$\mathbf{y}_k = C_k\mathbf{z}_k + D_k\mathbf{u}_k, \tag{4}$$

where $\Phi(k+1, k)$ is the state transition matrix between time steps. The system identification problem corresponds to finding an estimate of the discrete time system matrices, A_k, B_k, C_k, and D_k from time history of $\mathbf{u}_k$ and $\mathbf{y}_k$. After obtaining this model, subsequent analyses identify vibrational modes that occur during the structure's motion. This information can then be utilized during the development and execution of the spacecraft's mission. Ideally, this output data would come from the spacecraft itself, but in the absence of an experimental test-bed, a high fidelity spacecraft model is utilized. The basics of this model are detailed in the Section IV.

It is assumed that the vibrations of the flexible membrane are caused by the rigid body motion only. A specific type of ERA is preformed within this paper referred to as "Initial Condition ERA" (ERA/IC). This means the system matrices are identified from experimental data in which there is no input and a nonzero deflection of the structure at the initial time. Once a model is obtained via ERA/IC, it will be tested to observe its accuracy. Additionally, how the sensors' noise level affects the accuracy of the identified model is studied (identified meaning the state-space form obtained via ERA/IC).

III. Model Identification

A. Time-Varying ERA from Initial Condition Response

ERA is an algorithm that required experimental data from one of two types of experiments: i) zero-state initial condition with impulse input or nonzero-state initial condition with zero input [20]. Additionally, the classic approach provided a time-invariant model, while this paper aims to identify a time-varying model. Traditionally, the algorithm utilizes the impulse input to define "Markov parameters" which are system-unique parameters used in Hankel matrices to preform system identification. Singular-value decomposition is applied to the Hankel matrices and heavy matrix algebra leads to the identified/minimal system matrices $\hat{A}_k$, $\hat{B}_k$, $\hat{C}_k$, and $\hat{D}_k$.

As a result of preforming initial-condition response, Markov parameters lose their meaning. As a result of the system being time-varying, Hankel matrices are not defined, but instead a Hankel-like matrix is formed. This Hankel-like matrix is populated with raw output data rather than Markov parameters. Now, instead of identifying $\hat{A}_k$, $\hat{B}_k$, $\hat{C}_k$, and $\hat{D}_k$ matrices, matrices $\hat{A}_k$, $\hat{C}_k$, and $\hat{X}_{0_k}$ are identified instead. Note that $\hat{X}_{0_k}$ is a vector of initial conditions in the minimal-realization coordinate system. There are no $\hat{B}$ and $\hat{D}$ matrices to identify because there is no input. The response of a generic discrete system with no input and an arbitrary initial condition (may be nonzero) is

$$\mathbf{x}_{k+1} = A_k \mathbf{x}_k \tag{5}$$

$$\mathbf{y}_k = C_k \mathbf{x}_k. \tag{6}$$

The general solution of equations (5) and (6) can be written in terms of the state-transition matrix, Φ_k, as,

$$\mathbf{x}_k = \Phi(k, k_o)\mathbf{x}_0 \tag{7}$$

$$\mathbf{y}_k = C_k \Phi(k, k_o)\mathbf{x}_0 \tag{8}$$

where $\Phi(k, k_o)$ is defined as,

$$\Phi(k, k_o) = \begin{cases} A_{k-1}A_{k-1}...A_{k_0}, & \forall k > k_0 \\ I & k = k_0 \\ undefined, & \forall k < k_0. \end{cases} \tag{9}$$

A reduced-order model of the system is obtained by utilizing initial-condition time-varying ERA (TVERA/IC). The algorithm begins by defining a Hankel-like matrix, $\tilde{H}_k$, whose columns consist of M experimental data vectors. These M columns of output data are concatenated up to the $(k + p - 1)^{th}$ time step, where p and M are chosen to capture the order, n, of the system.

$$\tilde{H}_k^{(p,N)} = \begin{bmatrix} y_k^{\#1} & y_k^{\#2} & \cdots & y_k^{\#N} \\ y_{k+1}^{\#1} & y_{k+1}^{\#2} & \cdots & y_{k+1}^{\#N} \\ \vdots & \vdots & \ddots & \vdots \\ y_{k+p-1}^{\#1} & y_{k+p-1}^{\#2} & \cdots & y_{k+p-1}^{\#N} \end{bmatrix} \tag{10}$$

To obtain a minimum realization of the discrete system, a singular-value decomposition of the $\tilde{H}_k$ matrix is preformed,

$$\tilde{H}_k = O_k^{(P)} X_k^{(N)} = U_k \Sigma_k^{\frac{1}{2}} \Sigma_k^{\frac{1}{2}} V_k^T \tag{11}$$

$$= \begin{bmatrix} U_k^{(n)} & U_k^{(0)} \end{bmatrix} \begin{bmatrix} \Sigma_k^{(n)} & 0 \\ 0 & \Sigma_k^{(0)} \end{bmatrix} \begin{bmatrix} V_k^{(n)^T} \\ V_k^{(0)^T} \end{bmatrix} \tag{12}$$

$$\simeq U_k^{(n)} \Sigma_k^{n^{\frac{1}{2}}} \Sigma_k^{n^{\frac{1}{2}}} V_k^{(n)^T}. \tag{13}$$

It can then be shown that a minimum realization of the discrete system is given by

$$\hat{A}_k = \Sigma_{k+1}^{n^{\frac{1}{2}}} V_{k+1}^{(n)^T} V_k^{(n)} \Sigma_k^{n^{-\frac{1}{2}}} \tag{14}$$

$$\hat{C}_k = E^{(m)^T} U_k^{(n)} \Sigma_{k+1}^{n^{\frac{1}{2}}} \tag{15}$$

$$\hat{X}_0 = \Sigma_0^{n^{-\frac{1}{2}}} U_0^{(n)^T} \tilde{H}_0, \tag{16}$$

where $E^{(m)^T} = \begin{bmatrix} I_m & O_m & \ldots & O_m \end{bmatrix}$ and m is the number of outputs for each experiment. Equations (14)-(16) are utilized within equations (5) and (6) to iterate over time and produce output data. If the reduced-order model accurately represents the dynamics of the true system, then the outputs of the two match. Note that one can only identify the model until the time step $t_f - p$. Any time after $t_f - p$, the $\tilde{H}_k$ matrix cannot be filled out and thus a state-space realization cannot be obtained. This meaning, the larger the value of p, the less time the identified model is valid for. It should also be reiterated that the state vector obtained via ERA, **z**, is *not* the same as the reference state vector, **x**. Conversely, the output, **y**, is the same for both systems. The identified state vector, **z**, is assumed to have no physical significance.

B. Comparing Identified and Reference Eigenvalues

One can write a transformation from the traditional state vector, $\boldsymbol{x}$, to a new state vector, z, as

$$z_k = T_k \boldsymbol{x}_k, \tag{17}$$

where z is the minimal-realization coordinate-system state vector obtained via TVERA (also referred to as the "identified" or "minimal" state). Rewriting equation (5) in terms of z

$$\begin{aligned} z_{k+1} &= T_{k+1}^{-1} A_k T_k z_k \qquad (18)\\ &:= \hat{A}_k z_k. \qquad (19) \end{aligned}$$

Note here that, unlike in time-invariant systems, $\hat{A}_k$ is not a similarity transformation of A_k; it is a more generic, topological transformation of A_k. This implies that the system matrices $\hat{A}_k$ and A_k do not have the same eigenvalues at any arbitrary values of k. Because the system evolution takes place in two different coordinate systems, T_{k+1}, T_k, this leads the basis vectors for the initial time step and the final time step to be different [20]. One wishes to compare the eigenvalues of the true and identified system matrices for analysis purposes. This discrepancy can be corrected by applying the following correction to the system matrix

$$\tilde{\hat{A}}_k = O_k^{\dagger} O_{k+1} \hat{A}_k, \tag{20}$$

where $(.)^{\dagger}$ denotes a pseudo inverse [20]. Equation (20) shows the transformation for the identified system matrix, $\hat{A}_k$, but this transformation must be applied to the true system matrix, A_k, as well. After the above transformation is applied, the following occurs:

$$\begin{aligned} \tilde{\hat{A}}_k &= O_k^{\dagger} O_{k+1} \hat{A}_k \\ &= T_k^{-1} O_k^{\dagger} O_{k+1} T_{k+1} T_{k+1}^{-1} A_k T_k \\ &= T_k^{-1} \underbrace{O_k^{\dagger} O_{k+1} A_k}_{\tilde{A}_k} T_k \\ &= T_k^{-1} \tilde{A}_k T_k. \end{aligned}$$

After applying the correction from equation (20), the system matrices are similarity transformations of each other and their eigenvalues can be compared at each time step. If the true system is a time-varying, linear system then the true and identified eigenvalues should match post transformation. If the true system is nonlinear then the eigenvalues do not necessarily match.

IV. Numerical Results

A. Coupled Rigid and Flexible Body Model

As a motivating example for ERA, consider the vibrations of the spacecraft depicted in Figure 2. This is a conceptual design for a spacecraft whose main mission is the collection and redirection of solar energy for power-beaming purposes. The structure is modeled as a rigid frame with a flexible membrane clamped within. The coupled equations of motion are derived based on the Lagrangian formulation presented in [6, 8] and are omitted from this paper for brevity sake. Only the resulting equation of motion related to the motion of the membrane is necessary for this analysis. The reference frames and relevant vectors are depicted in Figure 2. The black $\{\hat{\imath}, \hat{\jmath}, \hat{k}\}$ frame is the inertial-reference frame and the red $\{\hat{b}_1, \hat{b}_2, \hat{b}_3\}$ frame is the body-fixed frame.

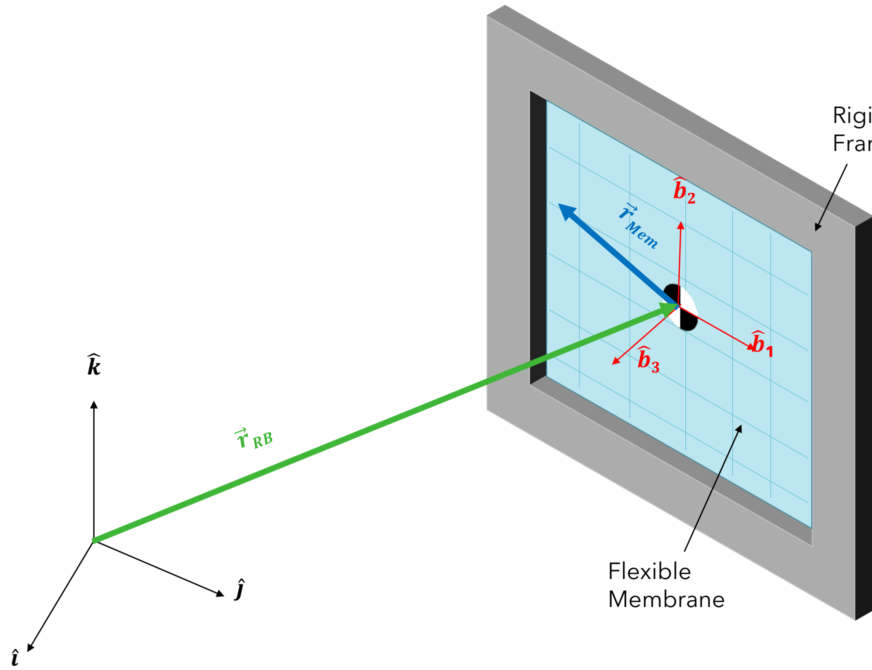

Figure 2 Spacecraft Model and Frame/Vector Definitions

1. Dynamics

The position vectors shown in Figure 2 are defined as

$$\mathbf{r}_{RB} = X\hat{\mathbf{b}}_1 + Y\hat{\mathbf{b}}_2 + Z\hat{\mathbf{b}}_3 \tag{21}$$

$$\mathbf{r}_{Flex} = \mathbf{r}_{RB} + \mathbf{r}_{Mem} \tag{22}$$

$$\mathbf{r}_{Flex} = \mathbf{r}_{RB} + x\hat{\mathbf{b}}_1 + y\hat{\mathbf{b}}_2 + \eta\hat{\mathbf{b}}_3 \tag{23}$$

$$= (X + x)\hat{\mathbf{b}}_1 + (Y + y)\hat{\mathbf{b}}_2 + (Z + \eta)\hat{\mathbf{b}}_3, \tag{24}$$

where {x,y,η} are the positions of any membrane element relative to the rigid body center of mass in the $\{\hat{\mathbf{b}}_1, \hat{\mathbf{b}}_2, \hat{\mathbf{b}}_3\}$ reference frame, respectively, and {X,Y,Z} are the inertial position of the center of mass of the rigid frame written in body-fixed coordinates.

The full set of differential equations of motion for the spacecraft are omitted from this paper for brevity's sake. For the purposes of this paper, the only necessary equation of motion is

$$\rho(\ddot{\boldsymbol{r}}_{Flex}) \cdot \boldsymbol{b}_3 - P\nabla^2\eta = \hat{f}. \tag{25}$$

Only using the above equation is sufficient for this analysis since the goal is to identify the vibrations of the membrane and not the rigid-body dynamics of the rigid frame. Note that ρ is the areal density of the membrane, P is the tension per unit length of the membrane, and $\hat{f}$ is an arbitrary distributed force applied to the membrane.

The displacement of the membrane normal to its surface, $\eta(x, y, t)$, is written as the double sum

$$\eta(x, y, t) = \sum_{i=1}^{n}\sum_{j=1}^{n} \phi_{ij}(x, y)q_{ij}(t), \tag{26}$$

where $\phi_{ij}(x, y)$ are the assumed modes, $q_{ij}(t)$ are the corresponding time-varying modal amplitudes, and $N \triangleq n^2$ is the total number of assumed modes. Two indices are needed since the membrane is a two-dimensional structure. The assumed modes are taken to be the eigenfunctions of a clamped-clamped membrane case and are defined as

$$\phi_{ij}(x, y) = \sin\left[\frac{i\pi}{a}(x - \frac{a}{2})\right] \sin\left[\frac{j\pi}{b}(y - \frac{b}{2})\right] \qquad i, j = 1, 2, ..., n, \tag{27}$$

where a and b are the membrane's width and height, respectively. Opting to write the above assumed modes with a single index, for the case of $n = 2$, the modes are referred to as $[1\ 2\ 3\ 4]$ instead of $[(1,1)(1,2)(2,1)(2,2)]$, respectively. This meaning

$$\phi_i(x, y) := \phi_{jk}(x, y) \qquad \text{where } i = n(j-1) + k,$$

where now $\phi_i(x, y)$ goes from 1 to n^2. Once again, $N \triangleq n^2$ and represents the total number of assumed modes.

Now, applying the above assumed modes approximation to the expanded form of equation (25) and applying the Galerkin method of weighted residuals [23] leads to

$$\begin{aligned}\int_{b_1}^{b_2}\int_{a_1}^{a_2}\Big[&\rho\dot{v}_3\phi_j + \rho\phi_i\ddot{q}_i\phi_j + \rho\dot{\omega}_1 y\phi_j - \rho\dot{\omega}_2 x\phi_j - \rho v_1\omega_2\phi_j + \rho(-\omega_2^2 - \omega_1^2)(\phi_i q_i \phi_j)\\ &+\rho\omega_3\omega_2 y\phi_j + \rho\omega_1 v_2\phi_j + \rho\omega_1\omega_3 x\phi_j - P\phi_{xx_i} q_i\phi_j - P\phi_{yy_i} q_i \phi_j - \hat{f}\phi_j\Big]dxdy = 0\\ &i = 1, 2, ..., N \qquad j = 1, 2, ..., N,\end{aligned} \tag{28}$$

where N is the number of assumed modes. In equation (28), $\{v_1, v_2, v_3\}$ are the inertial velocities written in the body-fixed coordinates and $\{\omega_1, \omega_2, \omega_3\}$ are the angular velocities written in the body-fixed coordinates. Note that in equation (28) repeated indices, such as $\phi_i\ddot{q}_i$, represent the full summation of the function that is being approximated with assumed modes, whereas ϕ_j represents each individual assumed mode being used as weighting functions in the Galerkin method of weighted residuals.

The system of equations defined in (28) can be rearranged into the form

$$M\ddot{\boldsymbol{q}} + K\boldsymbol{q} = F, \tag{29}$$

where M, K, and F are defined as

$$M_{ij} = \int_{b_1}^{b_2}\int_{a_1}^{a_2}\Big[\rho\phi_i\phi_j\Big]dxdy \tag{30}$$

$$K_{ij} = \int_{b_1}^{b_2}\int_{a_1}^{a_2}\Big[-\rho(\omega_1^2 + \omega_2^2)\phi_j - P(\phi_{xx_i} + \phi_{yy_i})\phi_j\Big]dxdy \tag{31}$$

$$F_j = \int_{b_1}^{b_2}\int_{a_1}^{a_2}\Big[\hat{f} + \rho(-\dot{v}_3 - \dot{\omega}_1 y + \dot{\omega}_2 x + v_1\omega_2 - \omega_3\omega_2 y - \omega_1 v_2 - \omega_1\omega_3 x)\Big]\phi_j dxdy, \tag{32}$$

where $M \in \mathbb{R}^{N\times N}$, $K \in \mathbb{R}^{N\times N}$, and $F \in \mathbb{R}^{N\times 1}$. Here, i and j represent the (i^{th}, j^{th}) element of each matrix and both go from 1 to N. Note that there is no repeated index here so there is no summation in these definitions.

2. State Space Model

By assuming free vibrations ($F = 0$), the resulting equations of motion of the spacecraft model can be converted into the following first-order, continuous, time-varying, linear system

$$\dot{\boldsymbol{x}} = A_c(t)\boldsymbol{x} \tag{33}$$

$$\boldsymbol{y} = C(t)\boldsymbol{x}, \tag{34}$$

where $\boldsymbol{x} = [\boldsymbol{q} \quad \dot{\boldsymbol{q}}]^\intercal \in \mathbb{R}^{2N\times 1}$ is the state vector, $\boldsymbol{y} \in \mathbb{R}^{m\times 1}$ is the output vector, and

$$A_c(t) = \begin{bmatrix} O^{N\times N} & I^{N\times N} \\ -M^{-1}K(t) & O^{N\times N}\end{bmatrix}, \tag{35}$$

where $I^{N\times N}$ and $O^{N\times N}$ are the identity and zero matrices, respectively. M and K are the mass and stiffness matrices, respectively. Note that the only time-varying aspect comes from the $(\omega_1^2 + \omega_2^2)$ term in the K matrix as shown in equation (31) (assuming membrane parameters are constant).

The output for this system is the acceleration of the membrane at m locations; representing m accelerometers distributed across the membrane. The acceleration output matrix $C(t)$ is determined by first writing equation (26) in terms of matrix multiplication with the modal amplitude vector $\boldsymbol{q}$

$$\boldsymbol{\eta}_m = \begin{bmatrix} \phi_1(x_1, y_1) & \dots & \phi_N(x_1, y_1) \\ \vdots & \ddots & \vdots \\ \phi_1(x_m, y_m) & \dots & \phi_N(x_m, y_m) \end{bmatrix} \boldsymbol{q}, \tag{36}$$

where $\boldsymbol{\eta}_m$ represents a vector of displacement at m locations on the membrane. Noting that only $\boldsymbol{q}$ is a function of time on the right-hand-side of the equation (36), taking two time derivatives and substituting for $\ddot{\boldsymbol{q}}$ from equation (29) with $F = 0$ yields

$$\ddot{\boldsymbol{\eta}}_m = -\begin{bmatrix} \phi_1(x_1, y_1) & \dots & \phi_N(x_1, y_1) \\ \vdots & \ddots & \vdots \\ \phi_1(x_m, y_m) & \dots & \phi_N(x_m, y_m) \end{bmatrix} M^{-1} K(t) \boldsymbol{q}. \tag{37}$$

Lastly, defining $\ddot{\boldsymbol{\eta}}_m$ as the output vector, $\boldsymbol{y}$, and rewriting with $\boldsymbol{x} = [\boldsymbol{q} \quad \dot{\boldsymbol{q}}]^\intercal$ leads to

$$\begin{aligned} \boldsymbol{y} &= -\begin{bmatrix} \phi_1(x_1, y_1) & \dots & \phi_N(x_1, y_1) & \mathbf{0}^{1xN} \\ \vdots & \ddots & \vdots & \vdots \\ \phi_1(x_m, y_m) & \dots & \phi_N(x_m, y_m) & \mathbf{0}^{1xN} \end{bmatrix} M^{-1} K(t) \boldsymbol{x} && (38) \\ &= C(t) \boldsymbol{x}, && (39) \end{aligned}$$

where $\mathbf{0}^{1xN}$ are rows of zeros to eliminate the $\dot{\boldsymbol{q}}$ portion of $\boldsymbol{x}$.

For this paper, it is assumed $n = 2$ and therefore $N = 4$. This implies $A_c \in \mathbb{R}^{8\times 8}$. Equations (33) and (34) can then be discretized as

$$\begin{aligned} \boldsymbol{q}_{k+1} &= A_k \boldsymbol{q}_k && (40) \\ \boldsymbol{y}_k &= C_k \boldsymbol{q}_k, && (41) \end{aligned}$$

by using $A_k = \Phi(k + 1, k)$.

3. Initial Conditions

In order to excited all modes of the system, the initial conditions are chosen to be linear combinations of all four assumed flexible body modes, which are the columns of the eigenvector matrix $\Phi = \left[\boldsymbol{\phi}_1, \boldsymbol{\phi}_2, \dots, \boldsymbol{\phi}_i, \dots, \boldsymbol{\phi}_{2N}\right]$ obtained from the characteristic equation $|A - \lambda_i|\ \phi_i$. The initial conditions are chosen to be

$$\boldsymbol{q}_{0_i} = r_1(\boldsymbol{\phi}_1 + \boldsymbol{\phi}_2) + r_2(\boldsymbol{\phi}_3 + \boldsymbol{\phi}_4) + r_3(\boldsymbol{\phi}_5 + \boldsymbol{\phi}_6) + r_4(\boldsymbol{\phi}_7 + \boldsymbol{\phi}_8) \quad i = 1, 2, \dots, R, \tag{42}$$

where r_1 through r_4 are random scalars drawn from a normal distribution and R is the number of initial conditions used. In the absence of a real input for TVERA/IC, the initial conditions act as a sort of input instead. Therefore, it is necessary to have at least 4 (N) initial conditions in order to have "rich" enough input for TVERA/IC to identify the system order correctly.

4. Stability of Analytical State-Space Model

Assuming that the geometry of the membrane results in the integral bounds being symmetric (i.e. the membrane is a square or rectangle so $a_1 = -a_2$ and $b_1 = -b_2$), the resultant mass and stiffness matrices are diagonal. One can verify by inspection that the mass matrix integral shown in equation (30) evaluates to zero when $i \neq j$ and evaluates to a nonzero number when $i = j$ for the assumed modes given in equation (27) (assuming ρ is a constant). Therefore, the mass matrix, M, is diagonal.

As for the stiffness matrix, first simplify equation (31) by using the definition of the assumed modes given in equation

(27). The terms ϕ_{xx_i} and ϕ_{yy_i} can be written as

$$\begin{aligned}\phi_{xx_i} &= \frac{-i^2\pi^2}{a^2}\sin\left[\frac{i\pi}{a}(x-\frac{a}{2})\right]\sin\left[\frac{j\pi}{b}(y-\frac{b}{2})\right]\\ &= \frac{-i^2\pi^2}{a^2}\phi_i\\ \phi_{yy_i} &= \frac{-j^2\pi^2}{b^2}\sin\left[\frac{i\pi}{a}(x-\frac{a}{2})\right]\sin\left[\frac{j\pi}{b}(y-\frac{b}{2})\right]\\ &= \frac{-j^2\pi^2}{b^2}\phi_i.\end{aligned}$$

This leading to K_{ij} being rewritten as

$$\begin{aligned}K_{ij} &= \int_{b_1}^{b_2}\int_{a_1}^{a_2}\underbrace{\left[-\rho(\omega_1^2+\omega_2^2)+P\pi^2\left(\frac{i^2}{a^2}+\frac{j^2}{b^2}\right)\right]}_{:=\psi(i,j,\omega_1,\omega_2)}\phi_i\phi_j dxdy\\ &= \int_{b_1}^{b_2}\int_{a_1}^{a_2}\psi\phi_i\phi_j dxdy.\end{aligned} \tag{43}$$

The variable ψ is not a function of the spatial variables x and y. Therefore, it can be treated as a constant during the integration. Looking at the integral in equation (43), it is of the same form as the integral of the mass matrix from equation (30). Thus, the stiffness matrix, K, is diagonal for the same reasons the mass matrix, M, is diagonal. Setting $i = j$ and taking ψ out of the integral in equation (43) leads to

$$K_{ii} = \psi\int_{b_1}^{b_2}\int_{a_1}^{a_2}\phi_i^2 dxdy. \tag{44}$$

Since M and K are diagonal, each diagonal element of K must be positive for the system to be stable. M and K being diagonal results in equation (29) consisting of N decoupled spring-mass systems for the modal amplitude vector $\boldsymbol{q}$. If any element of K is negative, a negative stiffness will occur and the corresponding modal amplitude will grow unbounded. Since the integral part of equation (44) will always evaluate to a positive number, the focus is shifted to observing when the value of ψ is less than zero:

$$\psi = -\rho(\omega_1^2+\omega_2^2)+P\pi^2\left(\frac{i^2}{a^2}+\frac{i^2}{b^2}\right)\leq 0 \tag{45}$$

$$\rho(\omega_1^2+\omega_2^2)\geq P\pi^2\left(\frac{i^2}{a^2}+\frac{i^2}{b^2}\right)$$

$$(\omega_1^2+\omega_2^2)\geq\frac{P\pi^2 i^2}{\rho}\left(\frac{1}{a^2}+\frac{1}{b^2}\right). \tag{46}$$

If the angular velocity of the spacecraft is too high, K has at least one negative element and at least one modal amplitude grows exponentially. If the angular velocity is not constant over time, then the system becomes unstable if equation (46) is true at any time instance. This instability is a function of the size, density, and tension of the membrane. This result concludes that previously developed analytical model [6] is valid for low angular velocities (relative to the membrane parameters).

B. Model Identification Results

Next, the numerical analysis where the system matrix, A, is a time-varying matrix is preformed. This is done by having a time-varying angular velocity. The output sensors consist of an evenly space 4×4 grid that starts 1 meter away from the edges of the membrane. This is visualized in Figure 3.

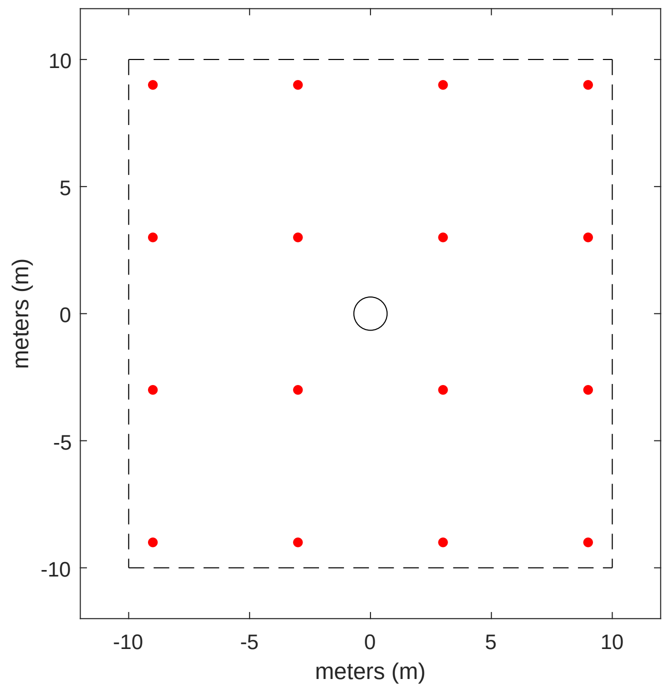

Figure 3 Sensor Layout: Red Dot Indicates Sensor, Black Circle Indicates Origin, and Black Dashed Line Indicates Membrane Border

For the results in this section, the following parameters are used

N	a	b	ρ	P	$\omega_1 = \omega_2$
4	10 m	10 m	$5\ \frac{\text{kg}}{\text{m}^2}$	$200\ \frac{\text{N}}{\text{m}}$	$0.001\ 0.01 sin(t) + 0.1\ \frac{\text{rad}}{\text{s}}$

along with the previously stated assumed modes. To obtain initial condition response data, the system is integrated at a propagation frequency of 100 Hz (i.e. $\Delta t = 0.01s$) and the data is sampled at every time step. The same random linear combination of the eigenvectors is used as an initial condition for all results. The time span used for TVERA/IC system identification is 0 to 20 seconds.

As for the sensor error, the noise is chosen to have a normal distribution with zero mean and a standard deviation equal to 1% of the max acceleration the membrane experienced (different for each initial condition case). For this experiment, $N = 20$ and $p = 5$ are used.

1. Singular Values of the Hankel-like Matrix

The singular values of the Hankel-like matrix at one time-instance are plotted in Figure 4. Note that, in general, the singular values will be time varying; however, all SVPs at each time instance had the same shape in this experiment. The blue data points correspond to the identified system with no noise, and the orange points to the system with noise. There are 8 dominate singular values for both cases and adding noise causes the non-dominate singular values to increase by approximately 13 orders of magnitude. The 8 values from both the noisy and no noise cases overlap in the figure. Note that 8 values are identified because the system matrix, A_k, is a $2N \times 2N$ matrix. Regardless, the true order of the system was determined accurately.

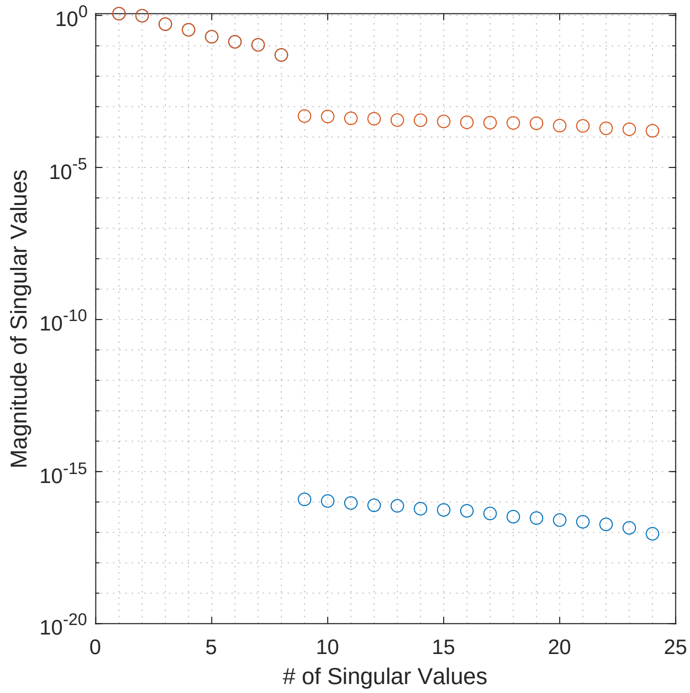

Figure 4 Singular Value Plot of Hankel-Like Matrix

2. Eigenvalue Comparison

To verify that the identified system is accurate, the eigenvalues of the identified system matrix, $\hat{A}_k$, are compared to the eigenvalues of the true system matrix, A_k. Figures 5 and 6 display the eigenvalues relative to the unit circle before and after the transformation derived in Section III.B. For both cases, the transformation clearly helped the ability to compare the eigenvalues. Subfigure (b) of each figure zooms in on one of the eigenvalue clusters after the transformation to provide a clearer view for comparison. The no-noise case very accurately reproduces the true eigenvalues. There is an interesting elliptical-like structure of the identified eigenvalues, while the true eigenvalues move purely on the unit circle. In the noisy case, the identified eigenvalues lose their elliptical structure and instead become more of a cloud around the true eigenvalues. Regardless, the identified eigenvalues accurately reproduce the true eigenvalues after the transformation is applied.

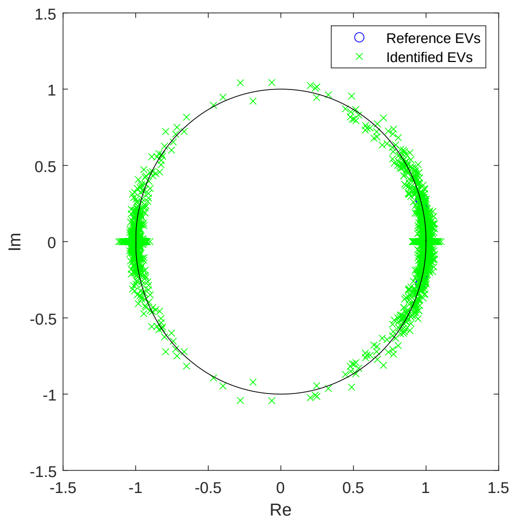

(a) Untransformed

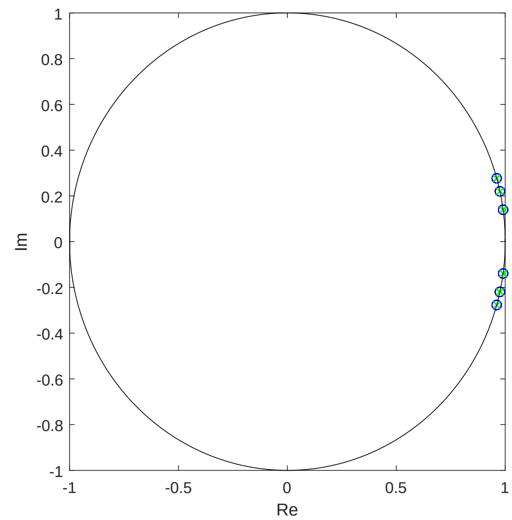

(b) Transformed

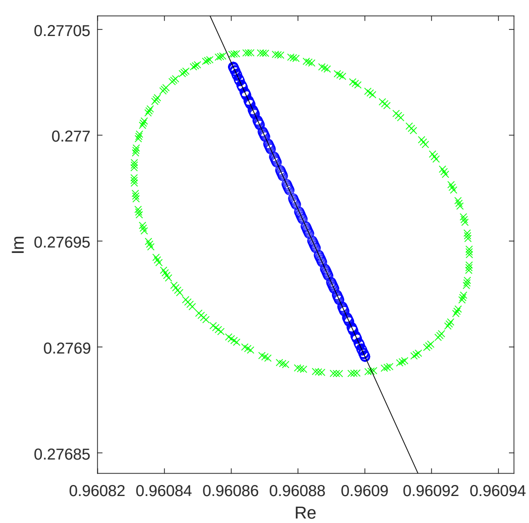

(c) Transformed: Zoomed View

Figure 5 Eigenvalue Comparison With No Noise

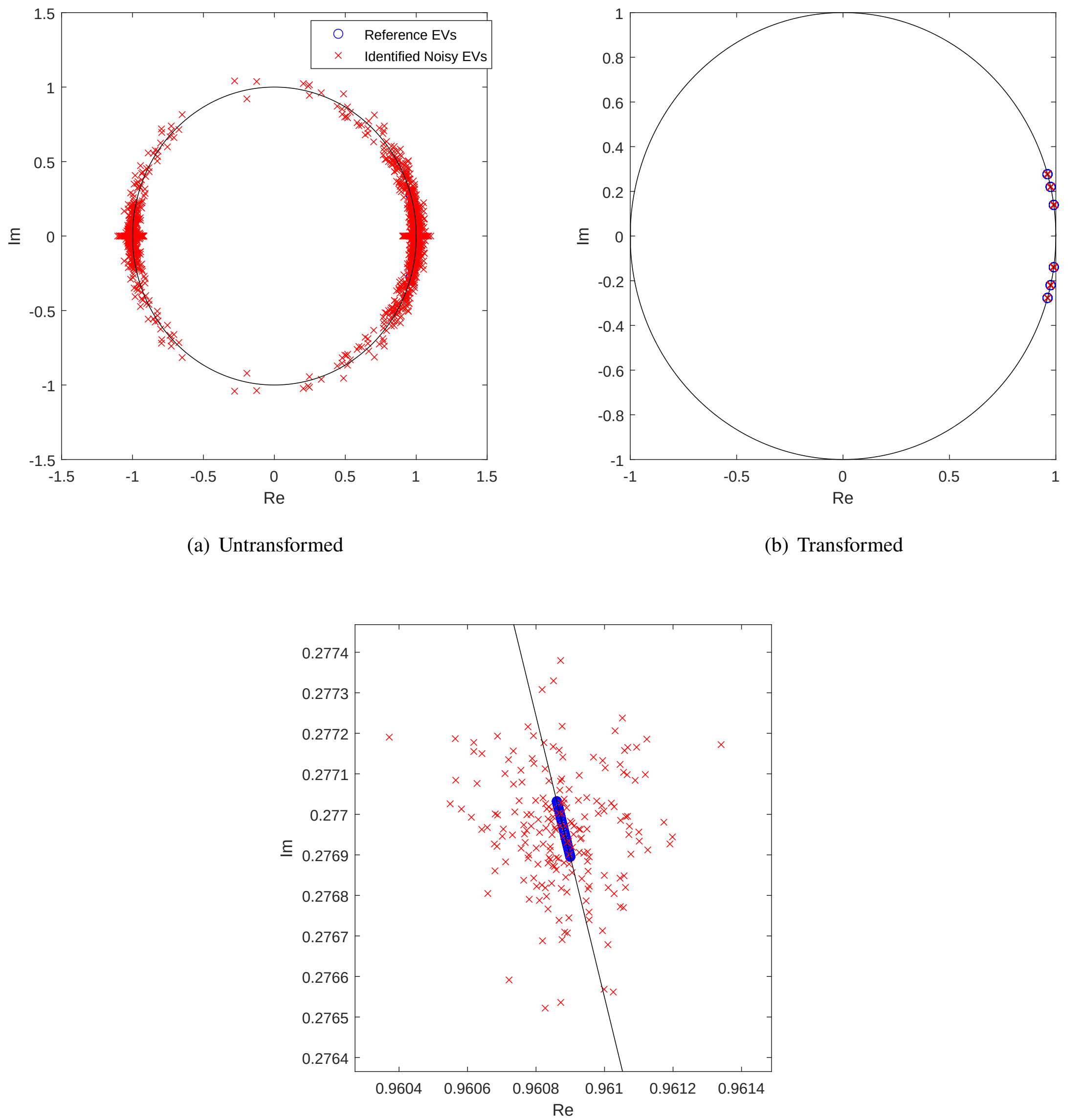

(a) Untransformed

(b) Transformed

(c) Transformed: Zoomed View

Figure 6 Eigenvalue Comparison With Sensor Noise

3. Verification

Next, the output data of the identified system is verified by propagating the state-space model with the initial conditions. This is shown in Figure 7. In this experiment, 20 different initial conditions are used for propagation. Not all initial conditions are shown to keep the figures a reasonable size. All data not shown have similar trends to those shown.

In the case of no sensor noise, the estimation error is on the order of 10^{-15} for all cases. When sensor noise is added, The magnitude of the error increases to 10^{-4}. It is expected that the error would increase with sensor noise. Nonetheless, the noisy sensors reproduce the output of the system well. Since the output of the system often came close to (or crossed) zero, percent-error graphs could not be provided because of misleading spikes in their magnitude.

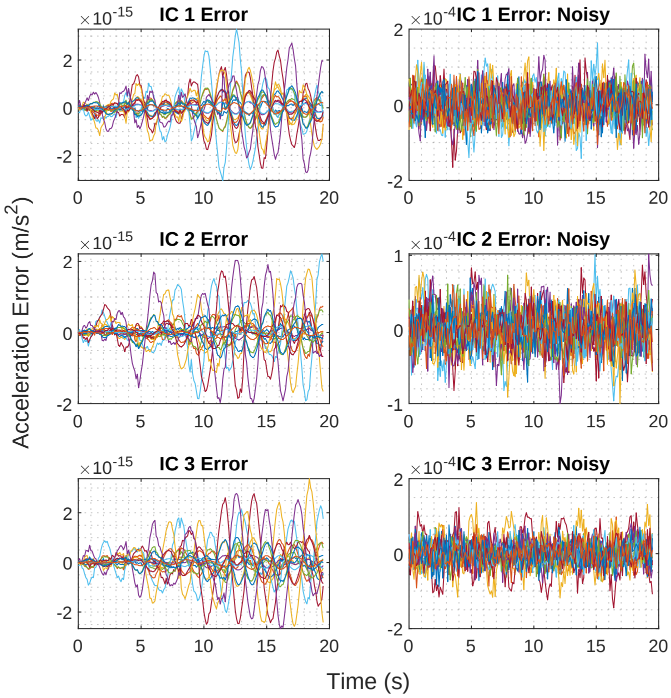

Figure 7 System-Output Replication Error

V. Conclusion

This paper demonstrates the efficacy of system identification algorithms in the dynamic modeling of large, flexible spacecraft. Previous work is utilized to obtain coupled rigid-flexible equations of motion for a large, flexible spacecraft via a Lagrangian method. Next, experimental response data is collected by propagating this high-fidelity dynamic model with nonzero initial conditions and zero input. ERA is then applied to obtain a minimal realization of the system matrices in the minimal coordinate system. This new system representation is then used to reproduce the high-fidelity model's dynamics. Accurate results are obtained from the reduced-order model and key dynamics are replicated even with sensor noise present.

Overall, this method provides an efficient and effective way to identify the dynamics of complex structures by analyzing the response from dominant modes. Combining the identified elastic model with known rigid-body dynamics yields an accurate, data-driven model. This is an invaluable tool in the analysis of hybrid space structures where analytical models sometimes fail to capture the dynamic coupling between the rigid and elastic domains. For spacecraft being used in the Space Solar Power Incremental Demonstrations and Research Project (SSPIDR), the pointing accuracy is of great importance. The solar energy collected must be directed accurately to the ground; therefore, a model that provides both high-accuracy of the structural vibrations, while keeping the computational complexity low, is required for mission success. This paper demonstrates that system identifications algorithms are practical and an excellent choice for solving this engineering problem. The results of this paper provide ground for exploring the reduced-order modeling of real, large, experimental space structures such as those inspired by SSPIDR.

VI. Acknowledgement

This material is based upon work federally funded by the Air Force Research Lab (AFRL) Scholars Program, AFRL SMART Scholarship, and AFOSR grant number FA9550-20-1-0176 P00001.

References

[1] "Space Solar Power Incremental Demonstrations and Research Project (SSPIDR)", afresearchlab.com/technology/successstories/space-power-beaming/

[2] "DSX (Cygnus)", https://space.skyrocket.de/doc_sdat/dsx.htm

[3] "What is solar sailing?", https://www.planetary.org/articles/what-is-solar-sailing

[4] "LightSail 2 solar sail is still soaring above Earth more than two years after launch", https://www.space.com/light-sail-2-solar-sail-still-flying-planetary-society

[5] J. Junkins and P. Singla, *Multi-Resolution Methods for Modeling and Control of Dynamical Systems*, Chapman & Hall, pp. 179-205, 2009.

[6] Brownell, M., Sinclair, A. J., Singla, P. "A Subspace Method for Shape Estimation of Flexible Spacecraft Membrane". AIAA SciTech 2022 Forum (p. 2378).

[7] Junkins, J. L., Singla, P., Griffith, T. D., & Henderson, T., *Orthogonal Global/Local Approximation in N-dimensions: Applications to Input-Output Approximation*, In 6th International Conference on Dynamics and Control of Systems and Structures in Space, Cinque-Terre, Italy.

[8] J. Junkins and Y. Kim, *Introduction to Dynamics and Control of Flexible Structures*, American Institute of Aeronautics and Astronautics, Inc., pp. 139-225, 1993.

[9] B. Ho and R. Kalman, *Effective Construction of Linear State Variable Models from Input/Output Data*, Proceedings of the 3rd Annual Allerton Conference on Circuit and System Theory, pp. 449-459, 1965.

[10] Meirovitch, L., and T. Stemple. "Hybrid equations of motion for flexible multibody systems using quasicoordinates." Journal of Guidance, Control, and Dynamics Vol 18 No. 4 (1995): 678-688.

[11] A. Tether, *Construction of Minimal Linear State-Variable Models from Finite Input-Output Data*, IEEE Transactions on Automatic Control, Vol. AC-15, No. 4, pp. 427-436, Aug. 1970

[12] Silverman, L.M., *Realization of Linear Dynamical Systems*, IEEE Transactions on Automatic Control, Vol. AC-16, No. 6, 1971, pp. 554-567.

[13] R. Rossen and L. Lapidus, *Minimum Realizations and System Modeling: I. Fundamental Theory and Algorithms*, AIChE Journal, Vol. 18, No. 4, July 1972, pp. 673-684.

[14] R. Rossen and L. Lapidus, *Minimum Realizations and System Modeling: II. Theoretical and Numerical Extensions*, AIChE Journal, Vol. 18, No. 5, Sept. 1972, pp. 881-892.

[15] J. Juang, *Applied System Identification*, Prentice Hall, Englewood Cliffs, NJ, 1994, pp. 121–227.

[16] J. Juang and R. Pappa, *An Eigensystem Realization Algorithm for Modal Parameter Identification and Model Reduction*, Journal of Guidance, Control, and Dynamics Vol. 8, No. 5, 1984.

[17] J. Turner and H. Chun, *Optimal Distributed Control of a Flexible Spacecraft During a Large-Angle Maneuver*, AIAA Journal of Guidance, Control, and Dynamics Vol. 7, No. 3, 1984.

[18] N. Osikowicz and P. Singla, *Model-based Control of Tendon-Actuated Tensegrity Robots*, AIAA Region I Student Conference, 2021.

[19] J. Juang, M. Phan, L. Horta, and R. Longman *Identification of Observer/Kalman Filter Markov Parameters: Theory and Experiments*, AIAA Journal of Guidance, Control, and Dynamics Vol. 16, No. 2, 1993.

[20] M. Majji, J. Juang, and J. Junkins, *Time-Varying Eigensystem Realization Algorithm*, AIAA Journal of Guidance, Control, and Dynamics Vol. 33, No. 1, 2010.

[21] P. Singla and J. L. Junkins, *Multi-Resolution Methods for Modeling and Control of Dynamical Systems*, Chapman & Hall/CRC, Boca Raton, FL, 2008.

[22] P. Singla, T. Henderson, J. L. Junkins, and J. Hurtado, *A Robust Nonlinear System Identification Algorithm using Orthogonal Polynomial Network*, AAS/AIAA Space Flight Mechanics Meeting - Spaceflight Mechanics 2005, AAS 05-163, Vol. 120, pp 983–1002, 2005.

[23] J. Petrolito, *Approximate Solutions of Differential Equations Using Galerkin's Method and Weighted Residuals*, International Journal of Mechanical Engineering Education, Vol. 28, No. 1, January 2000, pp 14–26.

[24] Hurtado, J. E. and Sinclair, A. J. *Hamel Coefficients for the Rotational Motion of a Rigid Body* Proceedings of the Royal Society of London. Series A: Mathematical, Physical and Engineering Sciences, vol. 460, no. 2052, pp. 3613–3630, Dec. 2004.

[25] Clive L. Dym and Irving H. Shames, *Solid Mechanics: A Variational Approach* A Variational Approach, McGraw-Hill Book Company, New York, 1973.